Radical chemistry in the Pearl River Delta: observations and modeling of OH and HO₂ radicals in Shenzhen 2018

Xinping Yang[1,2], Keding Lu[1,2,*], Xuefei Ma[1,2], Yue Gao[1,2], Zhaofeng Tan[3], Haichao Wang[4], Xiaorui Chen[1,2], Xin Li[1,2], Xiaofeng Huang[5], Lingyan He[5], Mengxue Tang[5], Bo Zhu[5], Shiyi Chen[1,2], Huabin Dong[1,2], Limin Zeng[1,2], Yuanhang Zhang[1,2,*]

[1]State Key Joint Laboratory of Environmental Simulation and Pollution Control, College of Environmental Sciences and Engineering, Peking University, Beijing, China

[2]State Environmental Protection Key Laboratory of Atmospheric Ozone Pollution Control, Peking University, Beijing, China

[3]Institute of Energy and Climate Research, IEK-8: Troposphere, Forschungszentrum Juelich GmbH, Juelich, Germany

[4]School of Atmospheric Sciences, Sun Yat-Sen University, Zhuhai, China

[5]Laboratory of Atmospheric Observation Supersite, School of Environment and Energy, Peking University Shenzhen Graduate School, Shenzhen, China

Correspondence to: Keding Lu (k.lu@pku.edu.cn), Yuanhang Zhang (yhzhang@pku.edu.cn)

Abstract. The ambient OH and HO₂ concentrations were measured continuously during the STORM (STudy of the Ozone foRmation Mechanism) campaign at the Shenzhen site, located in the Pearl River Delta in China, in autumn 2018. The diurnal maximum OH and HO₂ concentrations, measured by laser-induced fluorescence, were 4.5×10^6 cm⁻³ and 4.5×10^8 cm⁻³, respectively. The state-of-the-art radical chemical mechanism underestimated the observed OH concentration, similar to the other warm-season campaigns in China. The OH underestimation was attributable to the missing OH sources, which can be explained by the X mechanism. Good agreement between the observed and modeled OH concentrations was achieved when an additional numerical X equivalent to 0.1 ppb NO concentrations was added to the base model. The modeled HO₂ could reproduce the observed HO₂, indicating the HO₂ heterogeneous uptake on HO₂ chemistry was negligible. Photolysis reactions dominated the ROx primary production rate. The HONO, O₃, HCHO, and carbonyls photolysis accounted for 29%, 16%, 16%, and 11% during the daytime, respectively. The ROx termination rate was dominated by the reaction of OH + NO₂ in the morning, and thereafter the radical self-combination gradually became the major sink of ROx in the afternoon. The atmospheric oxidation capacity was evaluated, with a peak of 0.75×10^8 molecules cm⁻³ s⁻¹ around noontime. A strong positive correlation between O₃ formation rate and atmospheric oxidation capacity was achieved, illustrating the atmospheric oxidation capacity was the potential tracer to indicate the secondary pollution.

1 Introduction

Severe ambient ozone (O_3) pollution is one of China's most significant environmental challenges, especially in urban areas (Shu et al., 2020;Li et al., 2019;Wang et al., 2020;Ma et al., 2019b;Wang et al., 2017). Despite the reduction in emissions of O_3 precursors, O_3 concentration is increasing, especially in urban cities. The O_3 average trends for the focus megacity clusters are 3.1 ppb a^{-1}, 2.3 ppb a^{-1}, 0.56 ppb a^{-1}, and 1.6 ppb a^{-1} for North China Plain (NCP), Yangtze River Delta (YRD), Pearl River Delta (PRD), and Szechwan Basin (SCB), respectively (Li et al., 2019). The nonlinearity between O_3 and precursors illustrates that it is necessary to explore the cause of O_3 production. The tropospheric O_3 is only generated in the photolysis of nitrogen dioxide (NO_2), produced as the by-product within the radical cycling. Thus, the investigation of radical chemistry is critical to controlling secondary pollution.

Hydroxyl radicals (OH), the dominant oxidant, control the atmospheric oxidation capacity (AOC) in the troposphere. The OH radicals convert primary pollutants to secondary pollutants and are simultaneously transformed into peroxy radicals (HO_2 and RO_2). Within the interconvert of ROx (= OH, HO_2, and RO_2), secondary pollutants are generated, and thus the further exploration of radical chemistry is significant. The radical closure experiment, an effective indicator for testing our understanding of radical chemistry, has been conducted since the central role of OH radicals was recognized in the 1970s (Levy, 1971;Hofzumahaus et al., 2009). The underestimation of OH radicals at environments characterized by low nitrogen oxides (NO) and high volatile organic compounds (VOCs) has been identified (Lu et al., 2013;Lu et al., 2012;Tan et al., 2017;Tan et al., 2019;Yang et al., 2021;Hofzumahaus et al., 2009;Lelieveld et al., 2008;Whalley et al., 2011). New radical mechanisms involving unclassical OH regeneration have been proposed, including Leuven Isoprene Mechanism (LIM) and X mechanism (Peeters and Muller, 2010;Peeters et al., 2014;Peeters et al., 2009;Hofzumahaus et al., 2009). The LIM has been cooperated with the current mechanism and is still not sufficient to explain the OH missing sources. The X mechanism was identified several times, but the amount of the numerical species, X, varied in different environments, and the nature of X is unknown (Hofzumahaus et al., 2009;Lu et al., 2013;Lu et al., 2012;Tan et al., 2017;Tan et al., 2019;Yang et al., 2021). Therefore, further exploration of radical regeneration sources is necessary.

Owing to the strong photochemistry influenced by high temperatures, high O_3 pollution appeared to occur in YRD and PRD, especially in PRD (Ma et al., 2019b;Wang et al., 2017). Radicals, the dominant oxidant in the troposphere, has been measured during warm seasons in NCP (Yufa 2006, Wangdu 2014, and Beijing 2016), YRD (Taizhou 2018), SCB (Chengdu 2019), and PRD (Backgarden 2006, and Heshan 2014) in China (Lu et al., 2013;Lu et al., 2012;Tan et al., 2017;Tan et al., 2019;Yang et al., 2021;Tan et al., 2021). The radical observations in PRD, where the cities are suffering from severe O_3 pollution, have not been conducted since 2014, and thus the oxidation capacity here has not been clear in recent years. Therefore, we carried out a continuous comprehensive field campaign (STudy of the Ozone foRmation Mechanism - STORM) involving radical observations in Shenzhen, one of the megacities in PRD, in autumn 2018. Overall, the following will be reported in this study.

61   (1) The observed OH and HO$_2$ radicals, and the comparison between the observed and modeled radical concentrations.

62   (2) The exploration of the unclassical OH regeneration sources based on the experimental budget.

63   (3) The sources and sinks of radicals.

64   (4) The evaluation of AOC and the quantitative relationship between O$_3$ formation and AOC.

65   **2 Methodology**

66   **2.1 Measurement site and instrumentation**

67   The STORM campaign was conducted from September to October 2018 in Peking University Shenzhen Graduate School

68   (22°60 N, 113°97 E), in the west of Shenzhen, Guangdong province. As shown in Fig. 1, this site was located in the university

69   town, which was surrounded by residential and commercial areas. The northwest of the site is close to the Shenzhen Wildlife

70   Park, and the northeast is close to the Xili Golf Club (Yu et al., 2020). The Tanglang Mountain Park with active biogenic

71   emissions is located about 1 km southeast of the site.

72

73   **Figure 1: Geographical location and surrounding environmental conditions of the measurement site in STORM campaign (The**

74   **maps are from https://map.baidu.com).**

75   Most instruments were set up on the top of a four-story academic building (about 20 m). Besides HOx radicals measured by

76   the Peking University Laser-Induced Fluorescence system (PKU-LIF) (see the details in Sect. 2.2), a comprehensive set of

77   trace gases was conducted to support the exploration of the radical chemistry, including meteorological parameters

78   (temperature, pressure, relative humidity), photolysis frequency, and the trace gases (NO, NO$_2$, O$_3$, VOCs, *etc.*). Most of the

79   inorganic trace gases (O$_3$, CO, NO, NO$_2$, and SO$_2$) were simultaneously measured by two sets of instruments, and good

80   agreement was achieved within the uncertainty. VOCs (aldehydes, alkenes, aromatics, isoprene, and oxygenated VOCs

81   (OVOCs)) were measured using a gas chromatograph following a mass spectrometer (GC-MS). In addition, HONO and HCHO

82   were measured as well. Table S1 in the Supplementary Information describes the experimental details of the meteorological

83   and chemical parameters during this campaign.

2.2 The OH and HO₂ measurements

84

85   The OH and HO₂ radicals were measured by Peking University laser-induced fluorescence system (PKU-LIF) based on the

86   fluorescence assay by gas expansion (FAGE) technique. The principle has been reported in previous studies (Lu et al., 2012;Tan

87   et al., 2017;Heard and Pilling, 2003;Lu et al., 2013;Ma et al., 2019a;Tan et al., 2019;Tan et al., 2018;Yang et al., 2021), only a

88   brief description of the instrument is presented here.

89   In principle, OH resonance fluorescence is released in the OH excitation by a 308 nm pulsed laser, and then OH radicals are

90   detected directly. HO₂ radicals are converted into OH via NO, and then they are detected. The system contains a laser module

91   and a detection module. Ambient air was drawn into two independent, parallel, low-pressure (3.5 mBar) cells through two

92   parallel nozzles with 0.4 mm diameter pinhole. The OH radicals are excited into resonance fluorescence in the OH detection

93   cell and detected by micro-channel plate detectors (MCP). In the HO₂ detection cell, NO is injected and converts HO₂ to OH

94   radicals, which then are excited by the laser and release resonance fluorescence. Besides, an OH reference cell in which a large

95   OH concentration is generated by pyrolysis of water vapor on a hot filament is applied to automatically correct the laser

96   wavelength.

97   Owing to the failure of the reference cell in this study, the NO mixing ratios injected into the HO₂ cell were set to be higher

98   than that in other campaigns in China because the HO₂ cell needed to be used as a reference cell to correct laser wavelength.

99   Here, NO mixing ratios were switched between 10 ppm and 20 ppm. There was no obvious difference in HO₂ signals under

100   the above two NO mixing ratios, indicating that the interference of RO₂ to HO₂ measurements was negligible despite the higher

101   NO mixing ratio than other campaigns in China.

2.3 Closure experiment

102

103   As an effective tool to explore the atmospheric radical chemistry, the radical closure experiment can investigate the state-of-

104   the-art chemical mechanism because of the extremely short lifetime of radicals (Stone et al., 2012;Lu et al., 2019). A zero-

105   dimensional box model was used to conduct the radical closure experiment, and the overall framework was reported by Lu et

106   al. (2019). In this work, we conducted the radical closure experiment based on the Regional Atmospheric Chemical Mechanism

107   updated with the lasted isoprene chemistry (RACM2-LIM1), as Tan et al. (2017) described in detail. The model was

108   constrained to the measured meteorological, photolysis frequency, and the critical chemical parameters (CO, NO, NO₂, VOCs,

109   etc.). The H₂ and CH₄ mixing ratios were set to 550 ppb and 1900 ppb, respectively. The model was operated in time-dependent

110   mode with a 5-min time resolution, and a 2-d spin-up time was used to reach steady-state conditions for long-lived species.

111   As Lu et al. (2012) described, there are two types of radical closure experiment. One is the comparison of observed and

112   modeled radical concentrations, and the other is the comparison of radical production and destruction rates. The most

113   significant difference between the above is that the latter is conducted with the radical concentrations and k_{OH} constrained. The

114   comparison of radical production and destruction rates, also called radical experimental budget, can test the accuracy of the

115   state-of-the-art chemistry mechanisms based on the equivalent relationship between the radical production and destruction

116   rates. The production rates of OH, HO$_2$, and RO$_2$ radicals are quantified from all the known sources. The destruction rates of

117   HO$_2$ and RO$_2$ radicals are the sum of the known sources. The OH destruction rate can be directly calculated as the product of

118   the observed OH concentrations and the observed k_{OH} (Tan et al., 2019;Yang et al., 2021). The OH destruction rate is the total

119   sinks of OH radicals because of the direct k_{OH} observation, and thus the discrepancy between the OH destruction and production

120   rates denotes the missing OH sources. The detailed reactions and the reaction rate constants related to OH, HO$_2$, and RO$_2$

121   radicals can be found in Tan et al. (2019) and Yang et al. (2021).

122   **2.4 AOC evaluation**

123   The life time of the trace gases is controlled not only by the oxidant concentration but also by its second-order rate constant,

124   so the atmospheric oxidation capacity (AOC) proposed by Geyer et al. (2001) is most suitable to evaluate the relative

125   importance of each oxidant (Elshorbany et al., 2009). AOC is the core driving force of complex air pollution, and determines

126   the removal rate of trace gases and the production rates of secondary pollutants (Liu et al., 2021). As an effective indicator for

127   atmospheric oxidation intensity, the evaluation of AOC can provide crucial information on the atmospheric composition of

128   harmful and climate forcing species (Elshorbany et al., 2009). AOC is defined as the sum of the respective oxidation rates of

129   the pollutants via reactions with oxidants (Elshorbany et al., 2009;Geyer et al., 2001). According to the definition of AOC, it

130   can be calculated by the Eq. (1).

131    $$\text{AOC} = \sum_i k_{Y_i}[Y_i][X] \tag{1}$$

132   where Y_i are the pollutants (CO, NO, NO$_2$, and VOCs), X are the main atmospheric oxidants (OH, O$_3$, NO$_3$), and k_{Y_i} is the

133   bi-molecular rate constant for the reaction of Y_i with X. The higher AOC, the higher removal rate of the most pollutants, and

134   thus the higher production rate of secondary pollutants (Yang et al., 2020a). Simultaneous measurements of OH and the key

135   trace gases are available in the study. NO$_3$ concentration could be simulated by the box model with the observed parameters

136   constrained.

137   **3. Results**

138   **3.1 Meteorological and chemical conditions**

139   Figure 2 gives an overview of the meteorological and chemical parameters from 05 October to 28 October 2018, when OH

140   and HO$_2$ radicals were measured. The diurnal variations of the temperature (T), relative humidity (RH), $j(\text{O}^1\text{D})$, and $j(\text{NO}_2)$

141   followed a regular pattern from day to day. The overall meteorological conditions were characterized by high temperature

142   (about 20~30 ℃), high relative humidity (60~80%), and intensive radiation with $j(\text{O}^1\text{D})$ up to 2.0×10^{-5} s^{-1} and $j(\text{NO}_2)$ up to

143   6.0×10^{-3} s^{-1}. The relative humidity and photolysis-frequency in this autumn campaign were similar to those in the summer

144   campaign conducted at Chengdu site (Yang et al., 2021). The temperature in this campaign was lower than that at Chengdu

145   site, but similar to that in the autumn campaign at Heshan site located in PRD as well (Tan et al., 2019;Yang et al., 2021).

146   The concentration of CO showed weak diurnal variation, indicating there was the non-obvious accumulation of

147   anthropogenic emissions on a regional scale. NO concentration peaked at 12 ppb during morning rush hour when the traffic

148   emission was severe, and thereafter, O_3 concentration started to increase with the decreasing of NO concentration. The maxima

149   of O_3 hourly concentration were high up to 120 ppb. According to the updated National Ambient Air Quality Standard of China

150   (GB3095-2012), O_3 concentration exceeded the Class-II limit values (hourly averaged limit 93 ppb) on several days (6, 7, 8,

151   and 26 October) when the environmental condition was characterized by high temperature and low relative humidity. NO_2

152   concentration was high at night because of the titration effect of O_3 with NO.

153   Along with the high O_3 concentration on 6, 7, 8, and 26 October, high HCHO concentration was also recorded during the

154   corresponding periods, indicating HCHO was mainly produced as secondary pollutions because of the active photochemistry

155   in this campaign. Isoprene, mostly derived from biogenic emissions and mainly affected by temperature, peaked around

156   noontime. Tan et al. (2019) reported the median concentration of HCHO and isoprene concentrations were 6.8 ppb and 0.6 ppb

157   during 12:00-18:00 at Heshan site. Similarly, the median concentration of HCHO and isoprene concentrations in this study

158   were 4.9 ppb and 0.4 ppb during the corresponding periods, respectively. As a proxy for traffic intensity, the toluene to benzene

159   ratio (T/B), which is below 2, means the traffic emissions are the major sources of VOCs (Brocco et al., 1997). The T/B

160   gradually dropped from 07:00 until it reached the minimum value at 09:00, indicating traffic emission contributed more to

161   VOCs during morning rush hour than during other periods. However, the T/B, which varied within a range of 7-12, was above

162   2, and thus VOCs emission during this campaign was mainly from other sectors such as those involving solvent evaporation.

163
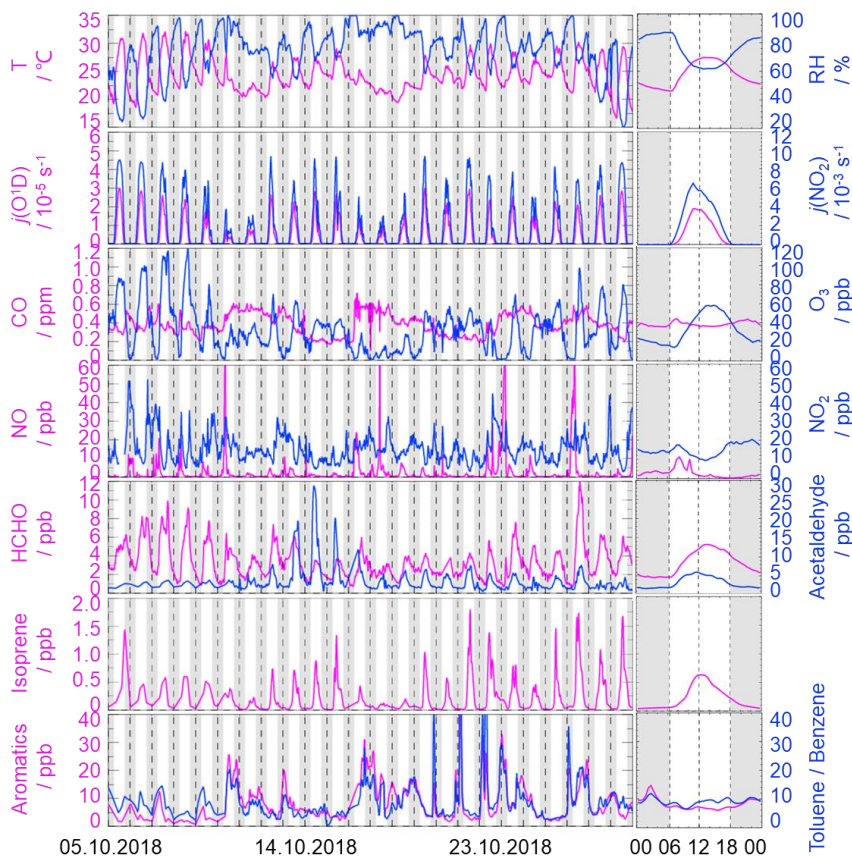
Figure 2: Timeseries and diurnal profiles of the observed meteorological and chemical parameters in STORM campaign. The grey areas denote nighttime.

3.2 Observed and modeled OH and HO₂ radicals

The OH and HO₂ radicals were measured during 05-28 October 2018. The timeseries of the observed and modeled HOx concentrations are displayed in Fig. S1 (a and b) in the Supplementary Information. Data gaps were caused by the rain, calibration, and maintenance. The daily maxima of the observed OH and HO₂ concentrations varied in the range of $(2-9) \times 10^6$ cm⁻³ and $(2-14) \times 10^8$ cm⁻³, respectively. As in previous campaigns, the largest OH concentrations appeared around noontime and showed a high correlation with $j(O^1D)$, a proxy for the solar UV radiation driving much of the primary radical production (Tan et al., 2019).

Figure 3 shows the diurnal profiles of the observed and modeled HOx concentrations (a and b). The HOx radicals showed similar diurnal behavior to those reported in other campaigns (Ma et al., 2019a;Tan et al., 2017;Tan et al., 2019;Tan et al., 2018;Yang et al., 2021). The observed OH and HO₂ concentration reached a maximum around 12:00 and 13:30, respectively. The diurnal maximum of the observed and modeled OH concentration was 4.5×10^6 cm⁻³ and 3.5×10^6 cm⁻³. There was an

177   agreement between the diurnal profiles of the observed and modeled OH concentrations within their errors of 11% and 40%,

178   respectively. A systematic difference existed with the decreasing of NO concentration. The model could reproduce the observed

179   OH concentrations well only in the early morning before 10:00. However, the model would underestimate the observed OH

180   concentration after 10:00 when NO concentration dropped 2 ppb. The OH concentrations observed in the environments with

181   low NO levels were underestimated by the state-of-the-art models at Backgarden (summer) and Heshan (autumn) sites in PRD

182   as well, and the OH underestimation was identified to be universal at low NO conditions in China (Lu et al., 2013;Lu et al.,

183   2012;Ma et al., 2019a;Tan et al., 2017;Yang et al., 2021).

184
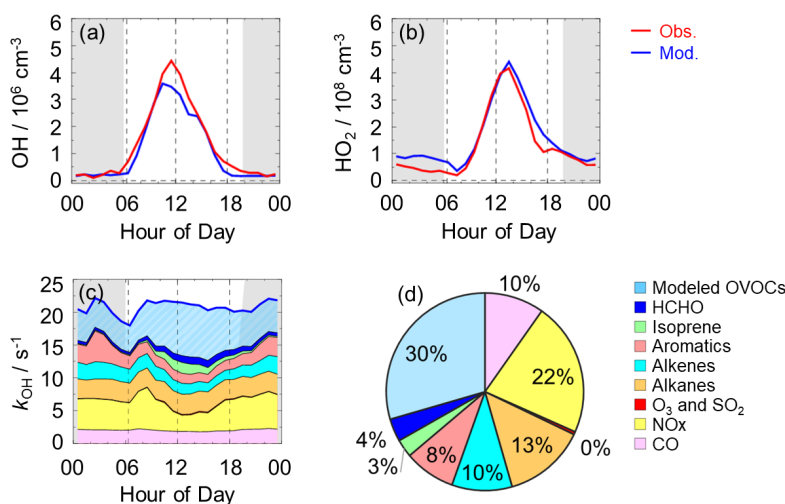
Figure 3: The diurnal profiles of the observed and modeled OH (a) and HO$_2$ (b) concentrations, the diurnal profiles of the modeled

185

k_{OH} (c), and the composition of the modeled k_{OH} (d). The grey areas denote nighttime.

186

187   The diurnal maximum of the observed HO$_2$ concentration was 4.5×10^8 cm^{-3}, and the modeled HO$_2$ concentration could

188   match well with the observed HO$_2$ concentration within the uncertainties, indicating the HO$_2$ heterogeneous uptake on HO$_2$

189   chemistry was negligible. The observed HO$_2$ concentration around noontime (11:00-15:00) was high, thereby yielding a mean

190   HO$_2$ to OH ratio (HO$_2$/OH) of about 112, which was similar to that at Backgarden site and was higher than that at Chengdu

191   site (Lu et al., 2012;Yang et al., 2021). The modeled HO$_2$/OH ratio was about 138. Prior studies indicated that the measured

192   HO$_2$/OH ratios were agreed well with the simulations under polluted conditions, but under clean conditions, the measured

193   ratios were lower than simulated (Stevens et al., 1997). The comparison of the measured HO$_2$/OH ratio and the modeled

194   HO$_2$/OH ratio in this campaign indicated the pollution was not severe during the observation period. As an indicator that can

195   reflect the interconversion reaction between OH and HO$_2$, the conversion efficiency in this campaign was equal to that at

196   Backgarden site and was slightly slower than that at Chengdu site.

3.3 Modeled k_{OH}

k_{OH} is the pseudo-first-order loss rate coefficient of OH radicals, and it is equivalent to the reciprocal OH lifetime (Fuchs et al., 2017;Lou et al., 2010;Yang et al., 2019). In this campaign, k_{OH} was not measured continuously, so we only showed the timeseries of modeled values in Fig. S1 (c) in the Supplementary Information, the diurnal profile of the modeled k_{OH} in Fig. 3 (c), and the composition of k_{OH} in Fig. 3 (d). The modeled k_{OH} showed weak diurnal variation and varied from 18 s^{-1} to 22 s^{-1}.

The inorganic compounds contributed approximately 32% to k_{OH}, in which the CO and NOx reactivity accounted for 10% and 22%, respectively. The NOx reactivity is displayed versus time, with a maximum during the morning peak. The peak concentration during the morning peak is associated with traffic emissions.

The larger fraction of k_{OH} comes from the VOCs group compared with inorganics reactivity, with a contribution of 68% to k_{OH}. OVOCs reactivity was equivalent to the other VOCs reactivity, and the contributions of them to k_{OH} were both 34%. The contribution of alkanes, alkenes, and aromatics were 13%, 10%, and 8%, respectively. The isoprene reactivity related to temperature was mainly concentrated during the daytime, whereas the aromatics reactivity at night was higher. As for OVOCs species, about 4% of k_{OH} could be attributed to HCHO. The remaining OVOCs was attributed to the simulated species in the box model, with a contribution of up to 30% of k_{OH}. High OVOCs reactivity occurred in the afternoon, which was attributed to the strong photochemical activity during this period.

4. Discussion

4.1 Radical closure experiment

In this study, we conducted OH radical closure experiment which is called OH experimental budget. The exploration of OH experimental budget was based on the premise that the modeled k_{OH} could matched well with the observed k_{OH} due to the lack of the continuous k_{OH} observations in this campaign. Several studies in China indicated that the modeled k_{OH} which has included OVOCs reactivity could match well with the observed k_{OH}, especially during daytime (Fuchs et al., 2017;Lou et al., 2010), but missing k_{OH} existed in some environmental conditions despite the inclusion of OVOCs (Whalley et al., 2021;Yang et al., 2017). Thus, the OH destruction rate is the lower limit due to the possible missing k_{OH} in this study, so the missing OH source, which is the difference between the OH destruction and production rates, is the lower limit as well. The diurnal profiles of OH production and destruction rates, and compositions of OH production rate were displayed in Fig. 4, with maxima of 14 ppb h^{-1} and 17 ppb h^{-1} around noontime, respectively. The OH production rate from known sources is quantified from the primary sources (photolysis of HONO, photolysis of O$_3$, ozonolysis of alkenes) and secondary sources (dominated by HO$_2$ + NO, and HO$_2$ + O$_3$). The primary and secondary sources were account for 78% and 22% of the total calculated production rate, respectively. Similar with the prior studies, the largest fraction of OH production rate comes from HO$_2$ + NO, with a contribution up to 76% of the known OH production rate. The contributions of HONO and O$_3$ photolysis were 13% and 7% to

227   the primary production rate.

228   The OH production rate matched well with the destruction rate only in the early morning to about 10:00. Thereafter, the OH

229   destruction rate was larger than the production rate, which could explain the underestimation of OH concentration by the model.

230   The discrepancy between the OH production and destruction rates was attributed the missing OH source. The biggest additional

231   OH source was approximately 4.6 ppb h^{-1}, which occurred at about 12:00, when the OH production and destruction rates were

232   11.9 ppb h^{-1} and 16.5 ppb h^{-1}, respectively. The unknown OH source could explain about one third of the total OH production

233   rate, indicating the exploration of missing OH source was significant to study the radical chemistry. Details are given below

234   (Sect. 4.2).
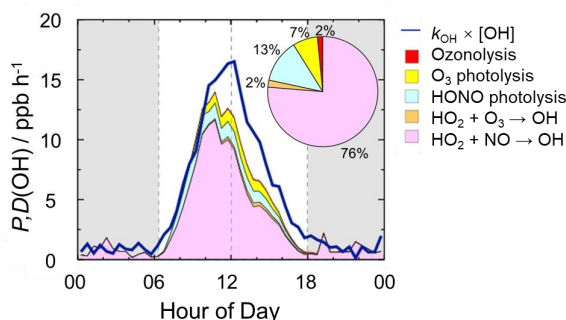
235

236   **Figure 4: The diurnal profiles of OH production and destruction rates and the proportions of different known sources in the**

237   **calculated production rate during the daytime. The blue line denotes the OH destruction rate, and the colored areas denote the**

238   **calculated OH production rates from the known sources. The grey areas denote nighttime.**

239   **4.2 Radical chemistry in low NO regime**

240   **4.2.1 Influencing factors of OH underestimation**

241   As analyzed in Sect. 4.1, the underestimation of OH concentration was attributable to the missing OH source. It is necessary

242   to explore the influencing factor for gaining further insight into the missing source. Scientists reported that more significant

243   OH underestimation would appear with the decreasing NO concentration and increasing isoprene concentration (Lu et al.,

244   2012;Ren et al., 2008;Hofzumahaus et al., 2009;Lelieveld et al., 2008;Whalley et al., 2011;Tan et al., 2017;Yang et al., 2021).

245   A new OH source was suggested, such as the LIM, which was proposed based on *ab inito* calculation (Peeters et al.,

246   2014;Peeters et al., 2009). We have applied the latest LIM into the base model in this study, and Tan et al. (2017) described

247   the modified LIM in detail. However, the model was not sufficient to explain the higher OH observations after 10:00.

248   We further explored the effect of NO concentration on missing OH source. NO dependence of OH and HO$_2$ radicals was

249   illustrated in Fig. 5. The base model can reproduce the observed OH concentration at high NO conditions (above 1 ppb) and

250   underestimate OH concentration at low NO conditions (below 1 ppb). As for HO$_2$ radical, the modeled HO$_2$ concentration by

251   the base model matched well with the observed HO$_2$ concentration within the whole NO regime. Therefore, NO concentration

252   played the significant role in the OH underestimation, especially under low NO regime.

253
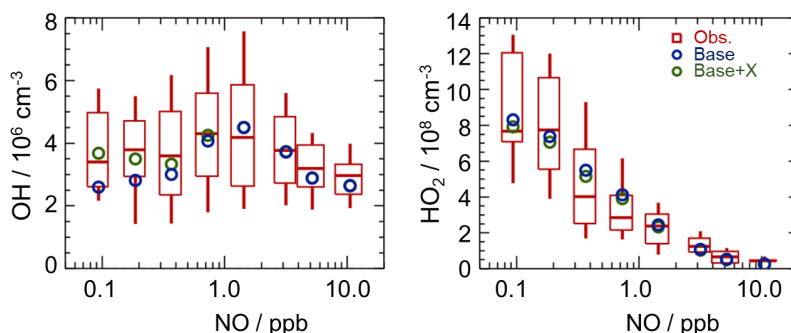
Figure 5: NO dependence of OH and HO₂ radicals. The red box-whisker plots give the 10%, 25%, median, 75%, and 90% of the HOx observations. The blue circles show the median values of the HOx simulations by the base model, and the green circles show the HOx simulations by the model with X mechanism. The OH concentrations were normalized by the averaged j(O1D) to eliminate the influence of radiation on the OH radicals. Only daytime values and NO concentration above the detection limit of the instrument were chosen.

4.2.2 Quantification of missing OH sources

260   Hofzumahaus et al. (2009) proposed an existence of a pathway for the regeneration of OH independent of NO, including the

261   conversions of $RO_2 \rightarrow HO_2$ and $HO_2 \rightarrow OH$ by a numerical species called X. With a retrospective analysis, the unclassical

262   OH recycling pathway was identified to be universal at low NO conditions in China. The amount of X varies with

263   environmental conditions, and the X concentrations were 0.85 ppb, 0.4 ppb, 0.1 ppb, 0.4 ppb, and 0.25 ppb at Backgarden,

264   Yufa, Wangdu, Heshan, and Chengdu sites (Hofzumahaus et al., 2009;Lu et al., 2012;Lu et al., 2013;Tan et al., 2017;Yang et

265   al., 2021).

266   In this study, we tested this unclassical X mechanism. Good agreement between observations and simulations of both OH

267   and HO₂ was achieved when a constant mixing ratio of 0.1 ppb of X was added into the base model. As shown in Fig. 5, the

268   model with X mechanism could agree with the observed OH concentrations even at low NO conditions. Unclassical OH

269   recycling was identified again in this study. However, X is an artificial species that behaves like NO, and thus the nature of X

270   is still unknown to us. Further exploration on this unclassical OH recycling is needed to improve our understanding of radical

271   chemistry.

4.3 Sources and sinks of ROx

273   The detailed analysis of radical sources and sinks was crucial to exploring radical chemistry. The experimental budget for HO₂

274   and RO₂ radicals could not be conducted because RO₂ was not measured during this campaign. Herein, we showed the

275   simulated results by the base model. Figure 6 illustrates the diurnal profiles of ROx primary production rate (P(ROx)) and

276   termination rate (L(ROx)), and the contributions of different channels during the daytime.
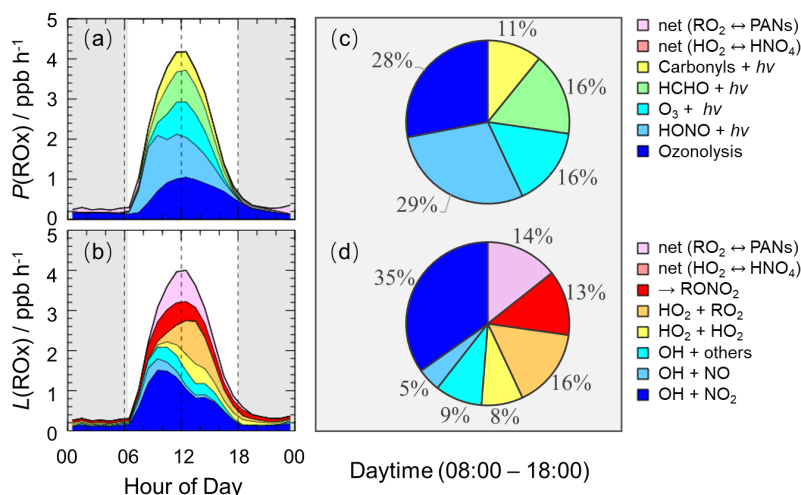
Figure 6: The diurnal profiles of ROx primary production rate (a) and termination rate (b) simulated by the base model, and the contributions of different channels to ROx primary production rate (c) and termination rate (d) during the daytime (08:00-18:00). The grey areas denote nighttime.

The ROx primary production and termination rates were basically in balance for the entire day, with maxima of 4 ppb h^{-1} around noontime. The ROx primary production rate was similar to those at Heshan (4 ppb h^{-1}) and Wangdu (5 ppb h^{-1}) sites, but lower than those at Backgarden (11 ppb h^{-1}), Yufa (7 ppb h^{-1}), and Chengdu (7 ppb h^{-1}) sites (Lu et al., 2013;Lu et al., 2012;Tan et al., 2017;Tan et al., 2019;Yang et al., 2021). During daytime, the main constitution of P(ROx) was OH and HO$_2$ primary production rate. HONO and O$_3$ photolysis mainly dominated the OH primary production rate, and HCHO photolysis constituted the major HO$_2$ primary production rate. P(ROx) was dominated by photolysis reactions, in which the photolysis of HONO, O$_3$, HCHO, and carbonyls accounted for 29%, 16%, 16%, and 11% during the daytime. In the early morning, HONO photolysis was the most important primary source of ROx, and the contribution of O$_3$ photolysis became progressively larger and was largest at noontime. A large discrepancy between the ratio of HONO photolysis rate to O$_3$ photolysis rate in summer/autumn and that in winter occurs generally. The vast majority of OH photolysis source is attributed to HONO photolysis in winter because of the higher HONO concentration and lower O$_3$ concentration. About half of L(ROx) came from OH termination, which occurred mainly in the morning, and thereafter, radical self-combination gradually became the major sink of ROx in the afternoon. OH + NO$_2$, OH + NO, and OH + others contributed 35%, 5%, and 9% to L(ROx), respectively. HO$_2$ + HO$_2$ and HO$_2$ + RO$_2$ accounted for 8% and 16% in L(ROx).

4.4 AOC evaluation

AOC controls the abundance of precursors and the production of secondary pollutants (Yang et al., 2020b;Elshorbany et al., 2009). It is necessary to quantify AOC for understanding photochemical pollution. The AOC has been evaluated in previous studies, as shown in Table 1. Overall, the AOC values in summer are higher than those in autumn and winter, and the values

299 at lower latitudes are higher than those at higher latitudes for the same reason. The vast majority of AOC in previous studies

300 are evaluated based on the non-observed radical concentrations.

301 **Table 1: Summary of OH concentrations and AOC values reported in previous field campaigns.**

Location	Season, year	Site	Observed or non-observed of OH radicals	AOC / 10^8 molecules cm^{-3} s^{-1}	References
Beijing, China	summer, 2018	urban	non-observed values	0.89[a]	(Liu et al., 2021)
Beijing, China	summer, 2018	suburban	non-observed values	0.85[a]	(Liu et al., 2021)
Beijing, China	winter, 2018	urban	non-observed values	0.21[a]	(Liu et al., 2021)
Beijing, China	winter, 2018	suburban	non-observed values	0.16[a]	(Liu et al., 2021)
Hongkong, China	summer, 2011	suburban	non-observed values	2.04[a,b]	(Xue et al., 2016)
Santiago, Chile	summer, 2005	urban	non-observed values	3.4[a]	(Elshorbany et al., 2009)
Hong Kong, China	late summer, 2012	coastal	non-observed values	1.4[c]	(Li et al., 2018)
Hong Kong, China	autumn, 2012	coastal	non-observed values	0.62[c]	(Li et al., 2018)
Hong Kong, China	winter, 2012	coastal	non-observed values	0.41[c]	(Li et al., 2018)
Shanghai, China	summer, 2018	urban	non-observed values	1.0[c]	(Zhu et al., 2020)
Berlin, Germany	summer, 1998	suburban	non-observed values	0.14[d]	(Geyer et al., 2001)
Xianghe, China	autumn, 2019	suburban	non-observed values	0.49[c]	(Yang et al., 2020b)
Beijing, China	summer, 2014	urban	non-observed values	1.7[a]	(Feng et al., 2021)

302 Note that:

303 [a] Peak values in the diurnal profiles; [b] Values on 25 August 2021; [c] Maximum over a period of time; [d] Maximum on some day.

304   Herein, we explored the AOC in Shenzhen based on the observed radical concentrations for the first time. As illustrated in

305 Fig. 7 (a), the diurnal profile of AOC exhibits a unimodal pattern, which is the same as the diurnal profile of OH concentration

306 and j(NO$_2$), with a peak around noontime. The diurnal peak of AOC was 0.75×10^8 molecules cm^{-3} s^{-1}. Comparatively, AOC

307 in this study can be comparable to those evaluated in Beijing (summer, 2018) and Hong Kong (autumn, 2012) (Li et al.,

308 2018;Liu et al., 2021), but much lower than those evaluated in Hong Kong (summer, 2011) and Santiago (summer, 2005) (Xue

309 et al., 2016;Elshorbany et al., 2009).
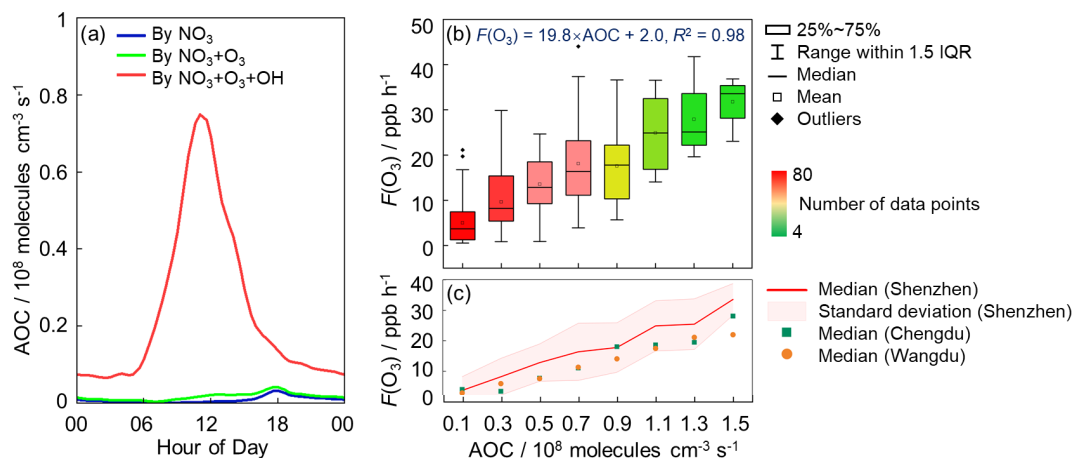
Figure 7: (a) The diurnal profiles of AOC in this campaign. (b) The correlation between F(O$_3$) and AOC during the daytime (08:00-18:00) in this campaign, and the formula was fitted by median values. (c) The comparison of the correlations between F(O$_3$) and AOC at this site, Wangdu site and Chengdu site.

As expected, the dominant contributor to the AOC during this campaign was OH, followed by O$_3$ and NO$_3$. Figure S2 shows the fractional composition of the total AOC. The OH radical contributed about 95.7% of AOC during the daytime (08:00-18:00). O$_3$, as the second important oxidant, accounted for only 2.9% of AOC during the daytime. The contribution of NO$_3$ to AOC during the daytime can be ignored, with a contribution of 1.4%. At night, the contributions of O$_3$ and NO$_3$ to AOC were higher. OH, O$_3$ and NO$_3$ accounted for 75.7%, 6.4%, and 18% in the first half of night (18:00-24:00), and they accounted for 87.8%, 5%, and 7.3% in the second half of night (00:00-08:00).

As an indicator for secondary pollution, O$_3$ formation rate, F(O$_3$), can be estimated from the production of NO$_2$ via the reactions of HO$_2$ and RO$_2$ with NO, as shown in Eq. (2).

$$F(O_3) = 9 \times 10^{-12}[HO_2][NO] + 9 \times 10^{-12}[RO_2][NO] \tag{2}$$

where the units of HO$_2$, RO$_2$, and NO are all cm^{-3}.

The correlation between F(O$_3$) and AOC during the daytime (08:00-18:00) was explored, as shown in Fig. 7 (b). A strong positive correlation between F(O$_3$) and AOC was found, indicating AOC plays a significant role in driving secondary pollution. Most data points in this campaign focused on low AOC (the median values below 0.7×10^8 molecules cm^{-3} s^{-1}) and low F(O$_3$) (the median values below 17 ppb h^{-1}) regimes. The correlation between F(O$_3$) and AOC by fitting the median was denoted by Eq. (3).

$$F(O_3) = 19.8 \times AOC + 2.0, R^2 = 0.98 \tag{3}$$

where the F(O$_3$) and AOC units are ppb h^{-1} and 10^8 molecules cm^{-3} s^{-1}, respectively.

To explore the correlation between F(O$_3$) and AOC in other regions, we have taken Wangdu and Chengdu sites as examples

332   to demonstrate the AOC values in NCP and SCB based on the observed radical concentrations reported by Tan et al. (2017)

333   and Yang et al. (2021) in Fig. 7 (c), respectively. Surprisingly, the relationships between $F(O_3)$ and AOC in Wangdu and

334   Chengdu were similar to those in the Shenzhen campaign. The vast majority of data points at Wangdu and Chengdu sites were

335   distributed within the standard deviation of Shenzhen site. The similarity of the gradients between $F(O_3)$ and AOC in different

336   regions indicates that AOC powerfully drives the production of O_3, and the quantification of $F(O_3)$ can be achieved based on

337   the AOC values.

338   **5 Conclusions**

339   The STORM field campaign was carried out at Shenzhen site in autumn 2018, providing the continuous OH and HO_2

340   observations in PRD since the Heshan campaign in 2014. The maximum diurnal OH and HO_2 concentrations, measured by

341   laser-induced fluorescence (LIF), were 4.5×10^6 cm^{-3} and 4.5×10^8 cm^{-3}, respectively. The observed OH concentration was

342   equal to that measured at Heshan site but was lower than those measured in summer campaigns in China (Backgarden, Yufa,

343   Wangdu, and Chengdu campaigns).

344   The base model (RACM2-LIM1) could reproduce the observed OH concentration before 10:00, and thereafter, OH was

345   underestimated by the model when NO concentration dropped to low levels. The results of the radical experimental budget

346   indicated that OH underestimation was likely attributable to an unknown missing OH source at low NO conditions. We

347   diagnosed the missing OH source by sensitivity runs, and unclassical OH recycling was identified again. A constant mixing

348   ratio of the numerical species, X, equivalent to 0.1 ppb NO, was added to the base model to achieve the agreement between

349   the modeled and observed OH concentrations. The amount of X related to the environmental conditions varied from 0.1 ppb

350   to 0.85 ppb in China, and thus the unclassical OH recycling needs further exploration. As for HO_2 radicals, good agreement

351   between the observed and modeled HO_2 concentrations was achieved for the entire day during this campaign, indicating the

352   HO_2 heterogeneous uptake on HO_2 chemistry was negligible.

353   The quantification of production and destruction channels of ROx radicals is essential to explore the chemical processes of

354   radicals. The ROx primary production and termination rates were balanced for the entire day, with maxima of 4 ppb h^{-1}, similar

355   to those in the Heshan and Wangdu campaigns. Photolysis channels dominated the ROx primary production rate. HONO, O_3,

356   HCHO, and carbonyls photolysis accounted for 29%, 16%, 16%, and 11% during the daytime, respectively. The most fraction

357   of ROx termination rate came from the reaction of OH + NO_2 in the morning. The radical self-combination gradually became

358   the major sink of ROx in the afternoon with the decreasing of NO concentrations. The reaction of OH + NO_2 and radical self-

359   combination accounted for 35% and 24% during the daytime, respectively.

360   In this campaign, AOC exhibited well-defined diurnal patterns, with a peak of 0.75×10^8 molecules cm^{-3} s^{-1}. As expected,

361   OH was the dominant oxidant accounting for 95.7% of the total AOC during the daytime. O_3 and NO_3 contributed 2.9% and

362   1.4% to total AOC during the daytime, respectively. The gradients at Shenzhen (PRD), Wangdu (NCP), and Chengdu (SBC)

363   sites were similar. The strong positive correlation between $F(O_3)$ and AOC makes the quantification of $F(O_3)$ achieved,

364   indicating AOC is the core driving force for the generation of secondary pollutants.

365

366   ***Data availability.*** The data used in this study are available from the corresponding author upon request (k.lu@pku.edu.cn).

367

368   ***Author contributions.*** YH Zhang and KD Lu conceived the study. XP Yang analyzed the data and wrote the manuscript with

369   inputs from KD Lu. XP Yang, XF Ma, Y Gao contributed to the measurements of the HOx concentrations. All authors

370   contributed to the discussed results and commented on the manuscript.

371

372   ***Competing interests.*** The authors declare that they have no conflict of interest.

373

374   ***Acknowledgment.*** The authors thank the science teams of the STORM-2018 campaign. This work was supported by the

375   Beijing Municipal Natural Science Foundation for Distinguished Young Scholars (JQ19031),the National Research Program

376   for Key Issue in Air Pollution Control (2019YFC0214800) , and the National Natural Science Foundation of China (Grants

377   No. 91544225, 21522701, 91844301).

378   **Appendix A. Supplementary data**

379   **References**

380   Brocco, D., Fratarcangeli, R., Lepore, L., Petricca, M., and Ventrone, I.: Determination of aromatic hydrocarbons in urban air
381   of Rome, Atmospheric Environment, 31, 557-566, 10.1016/s1352-2310(96)00226-9, 1997.

382   Elshorbany, Y. F., Kurtenbach, R., Wiesen, P., Lissi, E., Rubio, M., Villena, G., Gramsch, E., Rickard, A. R., Pilling, M. J., and
383   Kleffmann, J.: Oxidation capacity of the city air of Santiago, Chile, Atmospheric Chemistry and Physics, 9, 2257-2273,
384   10.5194/acp-9-2257-2009, 2009.

385   Feng, T., Zhao, S. Y., Hu, B., Bei, N. F., Zhang, X., Wu, J. R., Li, X., Liu, L., Wang, R. N., Tie, X. X., and Li, G. H.: Assessment
386   of Atmospheric Oxidizing Capacity Over the Beijing-Tianjin-Hebei (BTH) Area, China, Journal of Geophysical Research-
387   Atmospheres, 126, 18, 10.1029/2020jd033834, 2021.

388   Fuchs, H., Tan, Z., Lu, K., Bohn, B., Broch, S., Brown, S. S., Dong, H., Gomm, S., Haeseler, R., He, L., Hofzumahaus, A.,
389   Holland, F., Li, X., Liu, Y., Lu, S., Min, K.-E., Rohrer, F., Shao, M., Wang, B., Wang, M., Wu, Y., Zeng, L., Zhang, Y., Wahner,
390   A., and Zhang, Y.: OH reactivity at a rural site (Wangdu) in the North China Plain: contributions from OH reactants and
391   experimental OH budget, Atmospheric Chemistry and Physics, 17, 645-661, 10.5194/acp-17-645-2017, 2017.

392   Geyer, A., Alicke, B., Konrad, S., Schmitz, T., Stutz, J., and Platt, U.: Chemistry and oxidation capacity of the nitrate radical
393   in the continental boundary layer near Berlin, Journal of Geophysical Research-Atmospheres, 106, 8013-8025,
394   10.1029/2000jd900681, 2001.

395   Heard, D. E., and Pilling, M. J.: Measurement of OH and HO2 in the troposphere, Chemical Reviews, 103, 5163-5198,
396   10.1021/cr020522s, 2003.

397   Hofzumahaus, A., Rohrer, F., Lu, K., Bohn, B., Brauers, T., Chang, C.-C., Fuchs, H., Holland, F., Kita, K., Kondo, Y., Li, X.,
398   Lou, S., Shao, M., Zeng, L., Wahner, A., and Zhang, Y.: Amplified Trace Gas Removal in the Troposphere, Science, 324, 1702-
399   1704, 10.1126/science.1164566, 2009.
400   Lelieveld, J., Butler, T. M., Crowley, J. N., Dillon, T. J., Fischer, H., Ganzeveld, L., Harder, H., Lawrence, M. G., Martinez,
401   M., Taraborrelli, D., and Williams, J.: Atmospheric oxidation capacity sustained by a tropical forest, Nature, 452, 737-740,
402   10.1038/nature06870, 2008.
403   Levy, H.: NORMAL ATMOSPHERE - LARGE RADICAL AND FORMALDEHYDE CONCENTRATIONS PREDICTED,
404   Science, 173, 141-&, 10.1126/science.173.3992.141, 1971.
405   Li, K., Jacob, D. J., Liao, H., Shen, L., Zhang, Q., and Bates, K. H.: Anthropogenic drivers of 2013-2017 trends in summer
406   surface ozone in China, Proceedings of the National Academy of Sciences of the United States of America, 116, 422-427,
407   10.1073/pnas.1812168116, 2019.
408   Li, Z., Xue, L., Yang, X., Zha, Q., Tham, Y. J., Yan, C., Louie, P. K. K., Luk, C. W. Y., Wang, T., and Wang, W.: Oxidizing
409   capacity of the rural atmosphere in Hong Kong, Southern China, Science of the Total Environment, 612, 1114-1122,
410   10.1016/j.scitotenv.2017.08.310, 2018.
411   Liu, Z., Wang, Y., Hu, B., Lu, K., Tang, G., Ji, D., Yang, X., Gao, W., Xie, Y., Liu, J., Yao, D., Yang, Y., and Zhang, Y.:
412   Elucidating the quantitative characterization of atmospheric oxidation capacity in Beijing, China, Science of the Total
413   Environment, 771, 10.1016/j.scitotenv.2021.145306, 2021.
414   Lou, S., Holland, F., Rohrer, F., Lu, K., Bohn, B., Brauers, T., Chang, C. C., Fuchs, H., Haeseler, R., Kita, K., Kondo, Y., Li,
415   X., Shao, M., Zeng, L., Wahner, A., Zhang, Y., Wang, W., and Hofzumahaus, A.: Atmospheric OH reactivities in the Pearl
416   River Delta - China in summer 2006: measurement and model results, Atmospheric Chemistry and Physics, 10, 11243-11260,
417   10.5194/acp-10-11243-2010, 2010.
418   Lu, K., Guo, S., Tan, Z., Wang, H., Shang, D., Liu, Y., Li, X., Wu, Z., Hu, M., and Zhang, Y.: Exploring atmospheric free-
419   radical chemistry in China: the self-cleansing capacity and the formation of secondary air pollution, National Science Review,
420   6, 579-594, 10.1093/nsr/nwy073, 2019.
421   Lu, K. D., Rohrer, F., Holland, F., Fuchs, H., Bohn, B., Brauers, T., Chang, C. C., Haeseler, R., Hu, M., Kita, K., Kondo, Y.,
422   Li, X., Lou, S. R., Nehr, S., Shao, M., Zeng, L. M., Wahner, A., Zhang, Y. H., and Hofzumahaus, A.: Observation and modelling
423   of OH and HO2 concentrations in the Pearl River Delta 2006: a missing OH source in a VOC rich atmosphere, Atmospheric
424   Chemistry and Physics, 12, 1541-1569, 10.5194/acp-12-1541-2012, 2012.
425   Lu, K. D., Hofzumahaus, A., Holland, F., Bohn, B., Brauers, T., Fuchs, H., Hu, M., Haeseler, R., Kita, K., Kondo, Y., Li, X.,
426   Lou, S. R., Oebel, A., Shao, M., Zeng, L. M., Wahner, A., Zhu, T., Zhang, Y. H., and Rohrer, F.: Missing OH source in a
427   suburban environment near Beijing: observed and modelled OH and HO2 concentrations in summer 2006, Atmospheric
428   Chemistry and Physics, 13, 1057-1080, 10.5194/acp-13-1057-2013, 2013.
429   Ma, X., Tan, Z., Lu, K., Yang, X., Liu, Y., Li, S., Li, X., Chen, S., Novelli, A., Cho, C., Zeng, L., Wahner, A., and Zhang, Y.:
430   Winter photochemistry in Beijing: Observation and model simulation of OH and HO2 radicals at an urban site, Science of the
431   Total Environment, 685, 85-95, 10.1016/j.scitotenv.2019.05.329, 2019a.
432   Ma, X. Y., Jia, H. L., Sha, T., An, J. L., and Tian, R.: Spatial and seasonal characteristics of particulate matter and gaseous
433   pollution in China: Implications for control policy, Environmental Pollution, 248, 421-428, 10.1016/j.envpol.2019.02.038,
434   2019b.
435   Peeters, J., Nguyen, T. L., and Vereecken, L.: HOx radical regeneration in the oxidation of isoprene, Physical Chemistry
436   Chemical Physics, 11, 5935-5939, 10.1039/b908511d, 2009.
437   Peeters, J., and Muller, J.-F.: HOx radical regeneration in isoprene oxidation via peroxy radical isomerisations. II: experimental
438   evidence and global impact, Physical Chemistry Chemical Physics, 12, 14227-14235, 10.1039/c0cp00811g, 2010.
439   Peeters, J., Muller, J.-F., Stavrakou, T., and Vinh Son, N.: Hydroxyl Radical Recycling in Isoprene Oxidation Driven by
440   Hydrogen Bonding and Hydrogen Tunneling: The Upgraded LIM1 Mechanism, Journal of Physical Chemistry A, 118, 8625-
441   8643, 10.1021/jp5033146, 2014.
442   Ren, X., Olson, J. R., Crawford, J. H., Brune, W. H., Mao, J., Long, R. B., Chen, Z., Chen, G., Avery, M. A., Sachse, G. W.,
443   Barrick, J. D., Diskin, G. S., Huey, L. G., Fried, A., Cohen, R. C., Heikes, B., Wennberg, P. O., Singh, H. B., Blake, D. R., and

Shetter, R. E.: HOx chemistry during INTEX-A 2004: Observation, model calculation, and comparison with previous studies, Journal of Geophysical Research-Atmospheres, 113, 10.1029/2007jd009166, 2008.

Shu, L., Wang, T. J., Han, H., Xie, M., Chen, P. L., Li, M. M., and Wu, H.: Summertime ozone pollution in the Yangtze River Delta of eastern China during 2013-2017: Synoptic impacts and source apportionment, Environmental Pollution, 257, 10.1016/j.envpol.2019.113631, 2020.

Stevens, P. S., Mather, J. H., Brune, W. H., Eisele, F., Tanner, D., Jefferson, A., Cantrell, C., Shetter, R., Sewall, S., Fried, A., Henry, B., Williams, E., Baumann, K., Goldan, P., and Kuster, W.: HO2/OH and RO(2)/HO2 ratios during the Tropospheric OH Photochemistry Experiment: Measurement and theory, Journal of Geophysical Research-Atmospheres, 102, 6379-6391, 10.1029/96jd01704, 1997.

Stone, D., Whalley, L. K., and Heard, D. E.: Tropospheric OH and HO2 radicals: field measurements and model comparisons, Chemical Society Reviews, 41, 6348-6404, 10.1039/c2cs35140d, 2012.

Tan, Z., Fuchs, H., Lu, K., Hofzumahaus, A., Bohn, B., Broch, S., Dong, H., Gomm, S., Haeseler, R., He, L., Holland, F., Li, X., Liu, Y., Lu, S., Rohrer, F., Shao, M., Wang, B., Wang, M., Wu, Y., Zeng, L., Zhang, Y., Wahner, A., and Zhang, Y.: Radical chemistry at a rural site (Wangdu) in the North China Plain: observation and model calculations of OH, HO2 and RO2 radicals, Atmospheric Chemistry and Physics, 17, 663-690, 10.5194/acp-17-663-2017, 2017.

Tan, Z., Rohrer, F., Lu, K., Ma, X., Bohn, B., Broch, S., Dong, H., Fuchs, H., Gkatzelis, G. I., Hofzumahaus, A., Holland, F., Li, X., Liu, Y., Liu, Y., Novelli, A., Shao, M., Wang, H., Wu, Y., Zeng, L., Hu, M., Kiendler-Scharr, A., Wahner, A., and Zhang, Y.: Wintertime photochemistry in Beijing: observations of ROx radical concentrations in the North China Plain during the BEST-ONE campaign, Atmospheric Chemistry and Physics, 18, 12391-12411, 10.5194/acp-18-12391-2018, 2018.

Tan, Z., Lu, K., Hofzumahaus, A., Fuchs, H., Bohn, B., Holland, F., Liu, Y., Rohrer, F., Shao, M., Sun, K., Wu, Y., Zeng, L., Zhang, Y., Zou, Q., Kiendler-Scharr, A., Wahner, A., and Zhang, Y.: Experimental budgets of OH, HO2, and RO2 radicals and implications for ozone formation in the Pearl River Delta in China 2014, Atmospheric Chemistry and Physics, 19, 7129-7150, 10.5194/acp-19-7129-2019, 2019.

Tan, Z., Ma, X., Lu, K., Jiang, M., Zou, Q., Wang, H., Zeng, L., and Zhang, Y.: Direct evidence of local photochemical production driven ozone episode in Beijing: A case study, Science of the Total Environment, 800, 10.1016/j.scitotenv.2021.148868, 2021.

Wang, T., Xue, L. K., Brimblecombe, P., Lam, Y. F., Li, L., and Zhang, L.: Ozone pollution in China: A review of concentrations, meteorological influences, chemical precursors, and effects, Science of the Total Environment, 575, 1582-1596, 10.1016/j.scitotenv.2016.10.081, 2017.

Wang, W., Parrish, D. D., Li, X., Shao, M., Liu, Y., Mo, Z., Lu, S., Hu, M., Fang, X., Wu, Y., Zeng, L., and Zhang, Y.: Exploring the drivers of the increased ozone production in Beijing in summertime during 2005-2016, Atmospheric Chemistry and Physics, 20, 15617-15633, 10.5194/acp-20-15617-2020, 2020.

Whalley, L. K., Edwards, P. M., Furneaux, K. L., Goddard, A., Ingham, T., Evans, M. J., Stone, D., Hopkins, J. R., Jones, C. E., Karunaharan, A., Lee, J. D., Lewis, A. C., Monks, P. S., Moller, S. J., and Heard, D. E.: Quantifying the magnitude of a missing hydroxyl radical source in a tropical rainforest, Atmospheric Chemistry and Physics, 11, 7223-7233, 10.5194/acp-11-7223-2011, 2011.

Whalley, L. K., Slater, E. J., Woodward-Massey, R., Ye, C., Lee, J. D., Squires, F., Hopkins, J. R., Dunmore, R. E., Shaw, M., Hamilton, J. F., Lewis, A. C., Mehra, A., Worrall, S. D., Bacak, A., Bannan, T. J., Coe, H., Percival, C. J., Ouyang, B., Jones, R. L., Crilley, L. R., Kramer, L. J., Bloss, W. J., Vu, T., Kotthaus, S., Grimmond, S., Sun, Y., Xu, W., Yue, S., Ren, L., Acton, W. J. F., Hewitt, C. N., Wang, X., Fu, P., and Heard, D. E.: Evaluating the sensitivity of radical chemistry and ozone formation to ambient VOCs and NOx in Beijing, Atmospheric Chemistry and Physics, 21, 2125-2147, 10.5194/acp-21-2125-2021, 2021.

Xue, L., Gu, R., Wang, T., Wang, X., Saunders, S., Blake, D., Louie, P. K. K., Luk, C. W. Y., Simpson, I., Xu, Z., Wang, Z., Gao, Y., Lee, S., Mellouki, A., and Wang, W.: Oxidative capacity and radical chemistry in the polluted atmosphere of Hong Kong and Pearl River Delta region: analysis of a severe photochemical smog episode, Atmospheric Chemistry and Physics, 16, 9891-9903, 10.5194/acp-16-9891-2016, 2016.

Yang, X., Wang, H., Tan, Z., Lu, K., and Zhang, Y.: Observations of OH Radical Reactivity in Field Studies, Acta Chimica Sinica, 77, 613-624, 10.6023/a19030094, 2019.

491   Yang, X., Lu, K., Ma, X., Liu, Y., Wang, H., Hu, R., Li, X., Lou, S., Chen, S., Dong, H., Wang, F., Wang, Y., Zhang, G., Li, S.,
492   Yang, S., Yang, Y., Kuang, C., Tan, Z., Chen, X., Qiu, P., Zeng, L., Xie, P., and Zhang, Y.: Observations and modeling of OH
493   and HO2 radicals in Chengdu, China in summer 2019, The Science of the total environment, 772, 144829-144829,
494   10.1016/j.scitotenv.2020.144829, 2021.

495   Yang, Y., Shao, M., Kessel, S., Li, Y., Lu, K., Lu, S., Williams, J., Zhang, Y., Zeng, L., Noelscher, A. C., Wu, Y., Wang, X., and
496   Zheng, J.: How the OH reactivity affects the ozone production efficiency: case studies in Beijing and Heshan, China,
497   Atmospheric Chemistry and Physics, 17, 7127-7142, 10.5194/acp-17-7127-2017, 2017.

498   Yang, Y., Wang, Y., Yao, D., Zhao, S., Yang, S., Ji, D., Sun, J., Wang, Y., Liu, Z., Hu, B., Zhang, R., and Wang, Y.: Significant
499   decreases in the volatile organic compound concentration, atmospheric oxidation capacity and photochemical reactivity during
500   the National Day holiday over a suburban site in the North China Plain, Environmental Pollution, 263, 114657,
501   https://doi.org/10.1016/j.envpol.2020.114657, 2020a.

502   Yang, Y., Wang, Y., Yao, D., Zhao, S., Yang, S., Ji, D., Sun, J., Wang, Y., Liu, Z., Hu, B., Zhang, R., and Wang, Y.: Significant
503   decreases in the volatile organic compound concentration, atmospheric oxidation capacity and photochemical reactivity during
504   the National Day holiday over a suburban site in the North China Plain, Environmental Pollution, 263,
505   10.1016/j.envpol.2020.114657, 2020b.

506   Yu, D., Tan, Z., Lu, K., Ma, X., Li, X., Chen, S., Zhu, B., Lin, L., Li, Y., Qiu, P., Yang, X., Liu, Y., Wang, H., He, L., Huang,
507   X., and Zhang, Y.: An explicit study of local ozone budget and NOx-VOCs sensitivity in Shenzhen China, Atmospheric
508   Environment, 224, 117304, https://doi.org/10.1016/j.atmosenv.2020.117304, 2020.

509   Zhu, J., Wang, S., Wang, H., Jing, S., Lou, S., Saiz-Lopez, A., and Zhou, B.: Observationally constrained modeling of
510   atmospheric oxidation capacity and photochemical reactivity in Shanghai, China, Atmospheric Chemistry and Physics, 20,
511   1217-1232, 10.5194/acp-20-1217-2020, 2020.

512